AGU PUBLICATIONS

Journal of Advances in Modeling Earth Systems

RESEARCH ARTICLE
10.1002/2016MS000727

Exploring the impacts of physics and resolution on aqua-planet simulations from a nonhydrostatic global variable-resolution modeling framework

Chun Zhao[1], L. Ruby Leung[1], Sang-Hun Park[2], Samson Hagos[1], Jian Lu[1], Koichi Sakaguchi[1], Jinho Yoon[1,3], Bryce E. Harrop[1], William Skamarock[2], and Michael G. Duda[2]

[1]Atmospheric Sciences and Global Change Division, Pacific Northwest National Laboratory, Richland, Washington, USA, [2]National Center for Atmospheric Research, Boulder, Colorado, USA, [3]School of Earth Sciences and Environmental Engineering, Gwanju Institute of Science and Technology, Gwangju, South Korea

Key Points:
- Aqua-planet simulations from hydrostatic (H) and nonhydrostatic (NH) MPAS across multiple horizontal resolutions are analyzed
- Simulated precipitation, column integrated moisture, and large-scale circulation are less sensitive to resolution in NH-MPAS than H-MPAS
- Variable resolution simulation with NH-MPAS exhibits more zonally symmetric features in the refined region compared to that with H-MPAS

Correspondence to:
C. Zhao,
chun.zhao@pnnl.gov

Citation:
Zhao, C., et al. (2016), Exploring the impacts of physics and resolution on aqua-planet simulations from a nonhydrostatic global variable-resolution modeling framework, *J. Adv. Model. Earth Syst.*, *8*, 1751–1768, doi:10.1002/2016MS000727.

Received 30 MAY 2016
Accepted 4 OCT 2016
Accepted article online 20 OCT 2016
Published online 4 NOV 2016

Abstract The nonhydrostatic Model for Prediction Across Scales (NH-MPAS) provides a global framework to achieve high resolution using regional mesh refinement. Previous studies using the hydrostatic version of MPAS (H-MPAS) with the physics parameterizations of Community Atmosphere Model version 4 (CAM4) found notable resolution-dependent behaviors. This study revisits the resolution sensitivity using NH-MPAS with both CAM4 and CAM5 physics. A series of aqua-planet simulations at global quasiuniform resolutions and global variable resolution with a regional mesh refinement over the tropics are analyzed, with a primary focus on the distinct characteristics of NH-MPAS in simulating precipitation, clouds, and large-scale circulation features compared to H-MPAS-CAM4. The resolution sensitivity of total precipitation and column integrated moisture in NH-MPAS is smaller than that in H-MPAS-CAM4. This contributes importantly to the reduced resolution sensitivity of large-scale circulation features such as the intertropical convergence zone and Hadley circulation in NH-MPAS compared to H-MPAS. In addition, NH-MPAS shows almost no resolution sensitivity in the simulated westerly jet, in contrast to the obvious poleward shift in H-MPAS with increasing resolution, which is partly explained by differences in the hyperdiffusion coefficients used in the two models that influence wave activity. With the reduced resolution sensitivity, simulations in the refined region of the NH-MPAS global variable resolution configuration exhibit zonally symmetric features that are more comparable to the quasiuniform high-resolution simulations than those from H-MPAS that displays zonal asymmetry in simulations inside the refined region. Overall, NH-MPAS with CAM5 physics shows less resolution sensitivity compared to CAM4.

1. Introduction

Reliable climate prediction at regional scales remains one of the greatest challenges in climate change science [*IPCC*, 2013]. Although not a panacea for climate modeling [*NRC*, 2012], increasing model horizontal resolution has been shown to have some positive impacts on simulating regional climate [e.g., *Giorgi and Mearns*, 1991; *Giorgi and Marinucci*, 1996; *Leung et al.*, 2003; *Bacmeister et al.*, 2014]. Dynamical downscaling using nesting and stretched grid modeling has been used since the 1990s to achieve regional-scale simulations [*Wang et al.*, 2004]. More recently, it has become computationally feasible to perform global simulations at grid sizes of 25–50 km. For example, simulations at a horizontal resolution of ~25 km were used to study tropical cyclone changes in a warmer climate [*Murakami et al.*, 2010, 2012; *Roberts et al.*, 2015; *Wehner et al.*, 2014, 2015]. However, limited by computing resources, such simulations are still not routinely performed or considered standard in model intercomparison experiments. Through advances in grid generation techniques and numeric capability of handling distorted or nonorthogonal grids, global variable-resolution modeling offers an alternative approach for modeling regional climate at reduced computational cost compared to global uniform high-resolution modeling [e.g., *Medvigy et al.*, 2013; *Rauscher et al.*, 2013; *Zarzycki et al.*, 2014; *Sakaguchi et al.*, 2015]. Such modeling frameworks can also be used as an effective tool for assessing the resolution dependence or scalability of physical parameterizations [*Rauscher et al.*, 2013; *Hagos et al.*, 2013].

The Model for Prediction Across Scales (MPAS) is a variable-resolution model that uses unstructured spherical centroidal Voronoi tessellations (SCVTs) [*Du et al.*, 1999; *Ringler et al.*, 2008]. A single scalar density

function is used to generate global variable-resolution meshes with local refinement [e.g., *Ju et al*., 2011] over single or multiple high-resolution regions. The MPAS atmospheric dynamical core has been evaluated using the standard shallow-water test case suite of *Williamson et al*. [1992] for both quasiuniform [*Ringler et al*., 2010] and variable resolution [*Ringler et al*., 2011] meshes. The hydrostatic version of the MPAS dynamical core (H-MPAS) was coupled with the physics parameterizations of Community Atmosphere Model (CAM) version 4 (CAM4) [*Neale et al*., 2010] (H-MPAS-CAM4) [*Rauscher et al*., 2013] for climate simulations. H-MPAS-CAM4 has been evaluated in both idealized [*Rauscher et al*., 2013] and realistic [*Sakaguchi et al*., 2015] configurations. A series of studies have investigated the resolution sensitivity of H-MPAS-CAM4 in simulating the scaling behavior of clouds and precipitation [*O'Brien et al*., 2013], the structure of the intertropical convergence zone (ITCZ) [*Landu et al*., 2014], precipitation extremes [*Yang et al*., 2014], atmospheric river frequency [*Hagos et al*., 2015], and the position and strength of the eddy-driven jet [*Lu et al*., 2015].

The aforementioned studies have revealed notable resolution dependence in quasiuniform resolution aqua-planet simulations with H-MPAS-CAM4. For example, *Landu et al*. [2014] found a transition from a single to a double ITCZ as the MPAS mesh spacing is reduced from 240 to 30 km. The frequency of atmospheric rivers in the same set of simulations decreases dramatically with increasing model resolution that also shifts the subtropical jet poleward, reducing the likelihood of extratropical cyclones tapping tropical moisture [*Hagos et al*., 2015]. *Lu et al*. [2015] investigated the jet sensitivity to model resolutions using wave activity budgets and found a systematic weakening and poleward shift of the eddy-driven jet associated with the smaller effective diffusivity with increasing horizontal resolution. *Rauscher et al*. [2013] and *Hagos et al*. [2013] analyzed the zonally asymmetric circulation features in variable resolution H-MPAS-CAM4 aqua-planet simulations with a regional refinement over the tropics. They attributed the anomalous circulation to the enhanced precipitation downwind of the refined domain, and the Rossby waves excited by the anomalous diabatic heating [*Gill*, 1980]. The diverse resolution dependence behaviors found in these studies are partly attributable to the resolution-dependent physics parameterizations, particularly related to the moist processes, but the ability to better resolve the eddies as model resolution increases also plays an important role in simulations of large-scale features such as the jet stream. Arguably both factors as well as their interactions contribute importantly to the resolution-dependent performance of H-MPAS-CAM4, with implications for its effectiveness as a multiresolution modeling framework.

Parallel to the development of H-MPAS and its coupling with CAM4, *Skamarock et al*. [2012, 2014] developed a nonhydrostatic version of MPAS (NH-MPAS). Recently, the NH-MPAS dynamical core has been coupled with both CAM4 and CAM5 physics packages [*Neale et al*., 2010, 2012] (NH-MPAS-CAM4 and NH-MPAS-CAM5) in the Community Earth System Model (CESM) framework for climate research [*Park et al*., 2015]. This offers an opportunity to revisit the resolution dependence of MPAS to document whether and how the resolution sensitivity may differ in the two versions of MPAS dynamical cores and to evaluate the impacts of physics parameterizations, as the CAM4 and CAM5 physics packages feature important differences in cloud microphysics and turbulence parameterizations. Since previous studies have extensively explored the performance of H-MPAS-CAM4, this study will primarily highlight the distinct characteristics of NH-MPAS with CAM4 and CAM5 physics compared to H-MPAS-CAM4 in aqua-planet simulations. Analysis will focus on the physics and resolution impacts on simulated precipitation, clouds, and large-scale circulation.

The rest of the manuscript is organized as follows. Section 2 describes briefly the MPAS dynamical core, the CAM physics parameterizations, and the model setup for aqua-planet configuration. The series of aqua-planet experiments using NH-MPAS with CAM4 and CAM5 physics are analyzed in section 3, with comparison to the previous results from H-MPAS-CAM4. Comparisons are first discussed in the context of global quasiuniform resolution simulations at a range of horizontal resolutions, followed by analysis of global variable resolution simulations. The findings are then summarized in section 4.

2. Models and Experiments

2.1. MPAS-Atmosphere (MPAS-A) Dynamical Cores

The MPAS atmospheric dynamical core uses the horizontal C-grid scheme [*Thuburn et al*., 2009; *Ringler et al*., 2010] while the vertical and time discretization follows that of the Weather Research and Forecasting (WRF) model [*Skamarock et al*., 2008]. The MPAS-A hydrostatic and nonhydrostatic solvers are described in *Park*

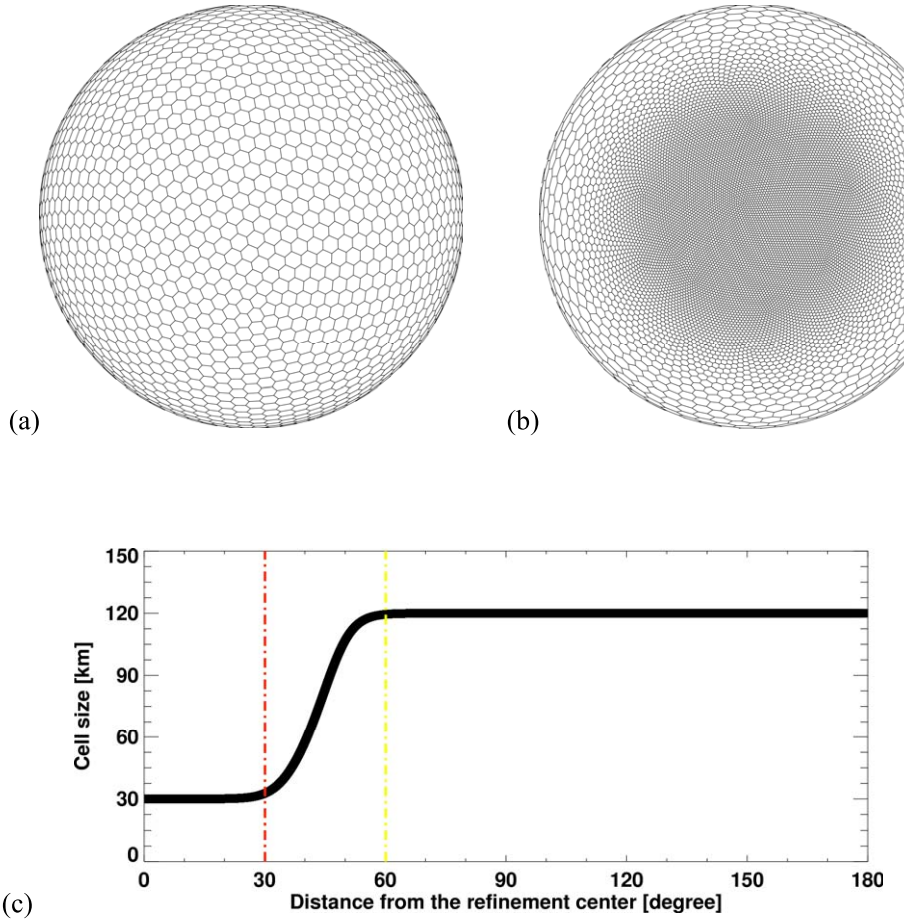

Figure 1. The (a) quasiuniform mesh and (b) variable-resolution mesh used in the UR and VR experiments. Both meshes are plotted at resolutions significantly lower than used in the experiments to show the mesh cells. (c) Mesh cell size as a function of distance from the refinement center (0°N, 0°E) in VR grid.

et al. [2013] and *Skamarock et al.* [2012], respectively. The most significant difference between the hydrostatic and nonhydrostatic atmospheric solvers is that H-MPAS uses a pressure coordinate while NH-MPAS uses a height coordinate. Thus, the vertical levels are necessarily different in the H-MPAS and NH-MPAS configurations in our experiments. More details about the hydrostatic hybrid-sigma coordinate and nonhydrostatic hybrid-height coordinate can be found in *Park et al.* [2013].

MPAS-A can be configured to use any refined meshes where the line segment connecting cell centers is orthogonal to the edge shared by the two cells. Figure 1 shows the quasiuniform and variable-resolution meshes used in this study, with the meshes coarsened to display the structure of the individual mesh cells. The quasiuniform mesh has essentially the same mesh spacing globally, while the variable-resolution mesh has finer mesh spacing in the refined region with a transition zone between the fine and coarse resolution meshes. More details about the mesh generation can be found in *Ringler et al.* [2011].

2.2. CAM Physics Parameterizations

The Community Atmosphere Model (CAM) is the atmospheric component of the Community Earth System Model (CESM). Implemented in the CESM framework, H-MPAS and NH-MPAS are coupled with both CAM4 and CAM5 physics packages in the same way as other dynamical cores in CESM [*Rauscher et al.*, 2013; *Park et al.*, 2015]. By default, CAM4 and CAM5 use 26 and 30 vertical levels, respectively. Both physics packages are tuned with respect to their own distributions of vertical levels, which should be considered intrinsic to each CAM physics package. More details about the physics-dynamics coupling and vertical level distributions in CESM with H-MPAS and NH-MPAS are described in *Park et al.* [2015]. Large differences exist in

Table 1. The Numbers of Grid Cells and Hyperdiffusion Coefficients ($m^4\ s^{-1}$) in the H-MPAS and NH-MPAS Experiments[a]

Resolution (km)	Number of Grid Cells	H-MPAS	NH-MPAS	Ratio (H/NH-MPAS)
240	10,242	5×10^{15}	6.91×10^{14}	7.24
120	40,962	5×10^{14}	8.64×10^{13}	5.79
60	163,842	5×10^{13}	1.08×10^{13}	4.63
30	655,362	5×10^{12}	1.35×10^{12}	3.70
30–>120	102,402	5×10^{12} to 5×10^{14} scaled	1.35×10^{12} to 8.64×10^{14} scaled	3.70–5.79 scaled

[a]The last column shows the ratio of hyperdiffusion coefficients between the H-MPAS and NH-MPAS experiments.

physics and chemistry parameterizations between CAM4 and CAM5. The CAM4 and CAM5 physics were described fully by *Neale et al*. [2010, 2012], respectively. Here, some relevant details are briefly summarized.

CAM4 uses the Rasch-Kristjánsson single moment bulk microphysics parameterization that prognoses cloud condensate (with liquid and ice as separate classes) and includes formulations of autoconversion, collection/accretion, and sedimentation [*Rasch and Kristjánsson*, 1998; *Neale et al*., 2010]. CAM5 uses the Morrison-Gettelman two-moment bulk microphysics parameterization [*Morrison and Gettelman*, 2008; *Gettelman et al*., 2008; *Neale et al*., 2012] that prognoses cloud condensate (with liquid and ice as separate classes) and cloud droplet number. It includes formulations of droplet activation, condensation-deposition, evaporation-sublimation, autoconversion, accretion, collection, sedimentation, homogenous and heterogeneous freezing, and ice melting. The Zhang [*Zhang et al*., 2003] and Park [*Neale et al*., 2012] macrophysics parameterizations are used in CAM4 and CAM5, respectively. The Zhang macrophysics parameterization calculates the stratiform, stratus, and convective cloud fraction separately, and diagnoses the total cloud fraction for a given grid cell as the convective cloud fraction plus the larger of the stratiform and stratus cloud fractions. The Park macrophysics parameterization does not calculate a separate stratus cloud fraction, and total fraction is calculated as the sum of the stratiform and convective cloud fractions. Both CAM4 and CAM5 use the modified *Zhang and McFarlane* [1995] deep convective parameterization [*Neale et al*., 2012]. However, CAM5 adopts a shallow convective scheme that uses a realistic plume dilution equation and closure to accurately simulate the spatial distribution of shallow convective activity [*Park and Bretherton*, 2009]. In addition, CAM4 uses a nonlocal transport scheme for the planetary boundary layer turbulence, while CAM5 uses a TKE moisture turbulence scheme [*Park and Bretherton*, 2009; *Neale et al*., 2012]. For chemistry, CAM4 uses the bulk aerosol scheme, while CAM5 uses a modal aerosol scheme [*Liu et al*., 2012; *Neale et al*., 2012]. In addition to online simulation of aerosols, both physics packages can be run with prescribed aerosol concentrations, which are used in our aqua-planet experiments.

2.3. Numerical Experiments

Following *Rauscher et al*. [2013], four different quasiuniform resolution (UR) meshes with mesh spacing of approximately 30, 60, 120, and 240 km and a variable resolution (VR) mesh, similar to that shown in Figure 1, have been configured. The VR mesh has a circular high-resolution region centered at the equator. The refined mesh has a radius of 30 degrees and a mesh spacing of approximately 30 km, with a transition zone of 30 degrees within which the mesh spacing gradually increases to approximately 120 km (Figure 1c). The numbers of grid cells of these meshes are listed in Table 1. The mesh spacing in these experiments resides in the hydrostatic regime. The same parameter values for the common physics schemes in CAM4 and CAM5 are used at multiple resolutions to explore the simulation sensitivity only to mesh resolution. Hence, the physics time step (10 min), dynamics time step (100 s), and moist-physics parameters are the same across all experiments that use the same physics. Following the hierarchical framework of *Leung et al*. [2013] and demonstrated by *Rauscher et al*. [2013] and *Hagos et al*. [2013], the UR experiments are used to quantify the impacts of horizontal resolution, while the VR experiments are mainly used to explore the potential of regional refinement for regional climate simulation.

The aqua-planet experiments are configured following *Neale and Hoskins* [2000] with SST distribution prescribed as follows:

$$T_s(\lambda,\phi)=\begin{cases} 27\left[1-\sin^2\left(\frac{3\phi}{2}\right)\right], & if -\frac{\pi}{3}<\phi<\frac{\pi}{3} \\ 0, & Otherwise \end{cases}$$

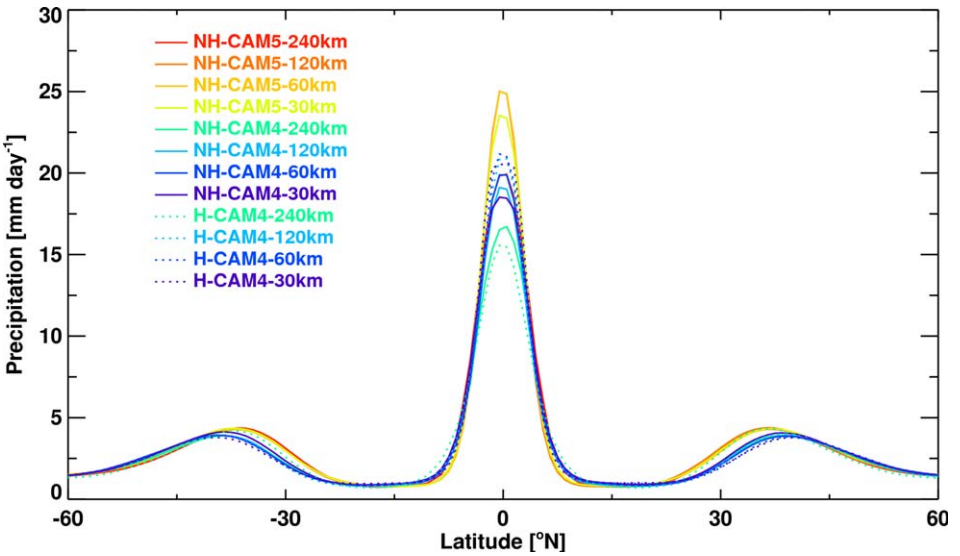

Figure 2. Zonal mean precipitation rates from the NH-MPAS simulations with CAM4 and CAM5 and the H-MPAS-CAM4 simulations at four different global quasiuniform resolutions of approximately 30, 60, 120, and 240 km. The results from simulations at various resolutions are all regridded to the 2° × 2° finite volume grid. Note that the result of NH-MPAS-CAM5 at 120 km mostly overlaps with the 60 km result.

Each simulation is run for 3 years, with the first 6 months discarded for spin-up, leaving 2.5 years for analysis. Some sensitivity experiments at coarser mesh spacing were extended to 5 years and the analysis results are comparable to those of the shorter simulations. The H-MPAS-CAM4 used in this study is the same model used in *Rauscher et al*. [2013], except for a bug fix in the interface between H-MPAS and the CAM4 physics that eliminated a small moisture imbalance between the global precipitation and evaporation found in the older version; its regional impact is visible only in the tropics. With this bug fix, our simulations show some differences from previously reported H-MPAS-CAM4 simulations [*Rauscher et al*., 2013], but the general model behaviors are largely comparable.

3. Results

3.1. Global Quasiuniform Resolution Simulations

3.1.1. Precipitation

Figure 2 shows the zonal mean precipitation rates from the UR NH-MPAS simulations with CAM4 and CAM5 physics and the UR H-MPAS-CAM4 simulations at approximately 30, 60, 120, and 240 km mesh spacing. Model outputs from simulations at various resolutions are all regridded to the 2° × 2° finite volume grid, but similar results are obtained using model outputs at the original resolution of each experiment. Since precipitation and its sensitivity to resolution beyond 60°N/S are subtle, only results between 60°N/S are shown in Figure 2. All simulations produce the highest precipitation at the equator (the ITCZ), with a secondary peak in the midlatitudes around 40°N/S corresponding to the storm tracks and a minimum in the subtropics. In *Rauscher et al*. [2013] and *Landu et al*. [2014], H-MPAS-CAM4 produced a single ITCZ at 120 and 240 km but a double ITCZ at 30 and 60 km. *Rauscher et al*. [2013] noted a dependence of the ITCZ structure on the model hyperdiffusion coefficient, as a sensitivity experiment with a smaller hyperdiffusion coefficient yielded a single ITCZ even at high resolution. *Landu et al*. [2014] attributed the double ITCZ feature in H-MPAS-CAM4 at high resolution to a feedback between convection and large-scale circulation. However, our simulations with H-MPAS and NH-MPAS all produce a single ITCZ regardless of model resolution. As discussed in section 2.3, the H-MPAS-CAM4 used in this study includes a bug fix that balances the global precipitation and evaporation more precisely. This results in increased atmospheric moisture in the simulations, as evidenced by the higher precipitation rate in our simulations compared to that reported previously at comparable resolutions [e.g., *Landu et al*., 2014; *Yang et al*., 2014]. Consistent with the mechanisms discussed in *Landu et al*. [2014], increased moisture increases the latent heat released by convection in the tropics. This induces larger upper tropospheric warming near the equator that increases poleward heat transport. The latter warms the upper troposphere and increases atmospheric stability poleward, limiting CAPE and the ITCZ to

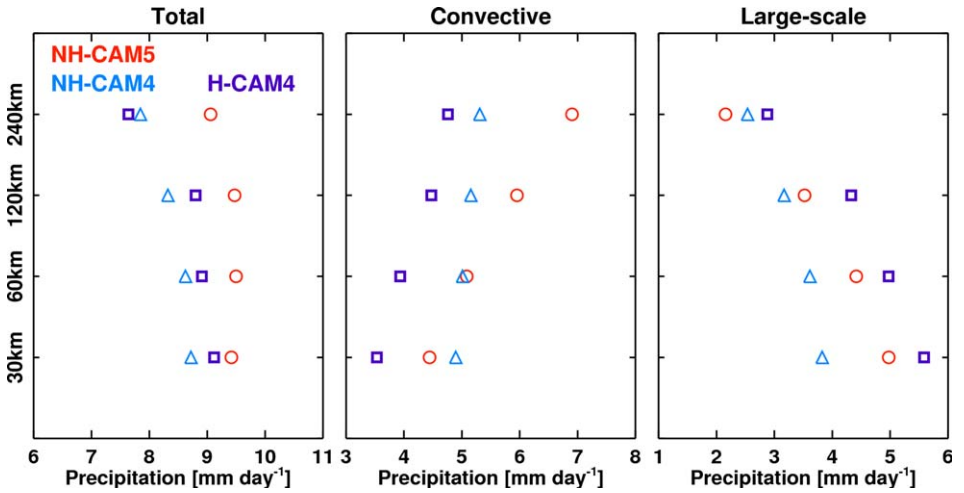

Figure 3. Mean tropical (10°S−10°N) total, parameterized convective, and resolved large-scale precipitation simulated at different resolutions by H-MPAS-CAM4 and NH-MPAS with CAM4 and CAM5 physics.

a narrower region centering about the equator. Hence, with the increased moisture resulting from the bug fix, H-MPAS-CAM4 produces a single ITCZ even at high resolution compared to the double ITCZ in the H-MPAS-CAM4 high-resolution simulations reported by *Landu et al*. [2014]. NH-MPAS simulates even higher moisture content than H-MPAS, so a single ITCZ is produced at all resolutions.

To better quantify the sensitivity of precipitation to resolutions and physics, Figure 3 shows the mean tropical (10°S–10°N) total, parameterized convective, and resolved large-scale precipitation simulated at different resolutions. As stronger updrafts are resolved with reduced mesh spacing, large-scale precipitation rates increase with increasing resolutions [*Williamson*, 2008a], while convective precipitation rates decrease as moisture is reduced by large-scale condensation. Hence, the ratio of convective to large-scale precipitation decreases with increasing resolutions. For NH-MPAS, this ratio is more sensitive to resolution with the CAM5 physics compared to the CAM4 physics. For the same physics (CAM4), H-MPAS generally simulates lower convective precipitation rates and higher large-scale precipitation rates than NH-MPAS at all resolutions, and the differences are larger at higher resolution.

Because of the opposite sensitivity of the simulated convective and large-scale precipitation rates to resolution in NH-MPAS-CAM5, the total precipitation increases only by a small amount of 4% (9.1–9.5 mm d^{-1}) with resolutions from 240 to 30 km, and is almost insensitive (9.4–9.5 mm d^{-1}) to resolutions from 120 to 30 km. The NH-MPAS-CAM4 simulated total precipitation is lower and more sensitive to resolution (11%, 7.8–8.7 mm d^{-1} from 240 to 30 km and 5%, 8.3–8.7 mm d^{-1} from 120 to 30 km) than NH-MPAS-CAM5. With CAM4 physics, the resolution sensitivity of total precipitation for H-MPAS and NH-MPAS is comparable, although the differences between the sensitivity of convective and large-scale precipitation to resolutions are large between H-MPAS and NH-MPAS. The sensitivity of the H-MPAS-CAM4 simulated total precipitation to resolution in this study is smaller than that reported by *Rauscher et al*. [2013], which is related to the moisture balance issue noted earlier. Overall, the total precipitation simulated in all experiments in this study is less sensitive to resolutions compared to the results in *Rauscher et al*. [2013].

In addition to the mean, the probability density functions (PDFs) of hourly tropical (10°S–10°N) precipitation for lower intensity events (0–150 mm d^{-1}, 1 mm d^{-1} bins) and higher intensity events (0–1000 mm d^{-1}, 10 mm d^{-1} bins) are shown in Figure 4. The results from simulations at various resolutions are all regridded to the $2^\circ \times 2^\circ$ grid. For lower intensity events (Figure 4a), it is evident that the coarser resolution simulations produce lower frequencies of more intense precipitation and higher frequencies of less intense precipitation compared to simulations at higher resolutions, with a transition occurring at around 45 mm d^{-1}. At the same resolution, CAM5 simulates higher frequencies of more intense precipitation than CAM4 in NH-MPAS, and H-MPAS-CAM4 simulates slightly higher frequencies of more intense precipitation than NH-MPAS-CAM4. Although the mean precipitation has weak sensitivity to resolution from 120 to 30 km (Figure 3), the impacts of resolution on the precipitation event frequencies are evident. The frequency distributions from simulations at 60 and 30 km are similar for NH-MPAS with CAM5 and CAM4.

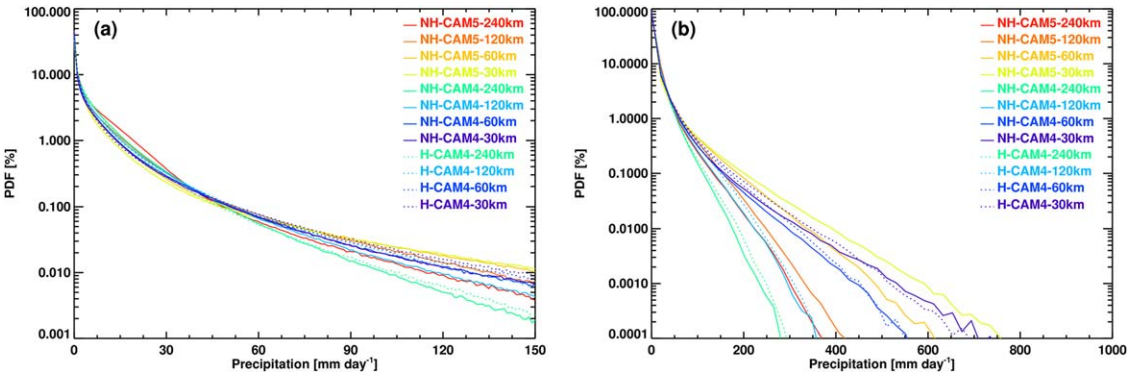

Figure 4. Probability density functions (PDFs) of hourly tropical (10°S−10°N) precipitation for (a) lower intensity events (0–150 mm d^{-1}, 1 mm d^{-1} bins) and (b) higher intensity events (0–1000 mm d^{-1}, 10 mm d^{-1} bins).

For higher intensity events (Figure 4b), resolution has significant impacts on extreme events even from 60 to 30 km. The NH-MPAS-CAM5 simulations produce higher frequencies of extreme precipitation than NH-MPAS-CAM4. The results from H-MPAS-CAM4 and NH-MPAS-CAM4 are similar. Overall, resolution has significant impacts on precipitation intensity, especially for the low probability-high intensity events, with no sign of convergence even at 30 km resolution, and simulations with CAM5 physics produce more intense precipitation than CAM4. Figure 5 shows the PDFs of 6 hourly tropical (10°S–10°N) upward vertical velocity averaged below 700 hPa. In general, the PDFs of extreme precipitation are consistent with those of upward vertical velocity. The figure shows that NH-MPAS-CAM5 produces higher frequencies of stronger updrafts than NH-MPAS-CAM4. The distributions of vertical velocity from H-MPAS-CAM4 and NH-MPAS-CAM4 are similar with slightly more frequent extreme updrafts in the former. The differences in vertical coordinate between NH-MPAS and H-MPAS and vertical resolution between CAM4 and CAM5 may contribute partly to their differences in PDFs of vertical velocity.

3.1.2. Large-Scale Circulation

3.1.2.1. Westerly Jet

Figure 6 shows the climatologically and zonally averaged zonal winds from the UR NH-MPAS simulations with CAM4 and CAM5 physics and the UR H-MPAS-CAM4 simulations at 240 km and the difference between 240 km and other resolutions. The general circulation pattern is similar to that reported in *Rauscher et al.*

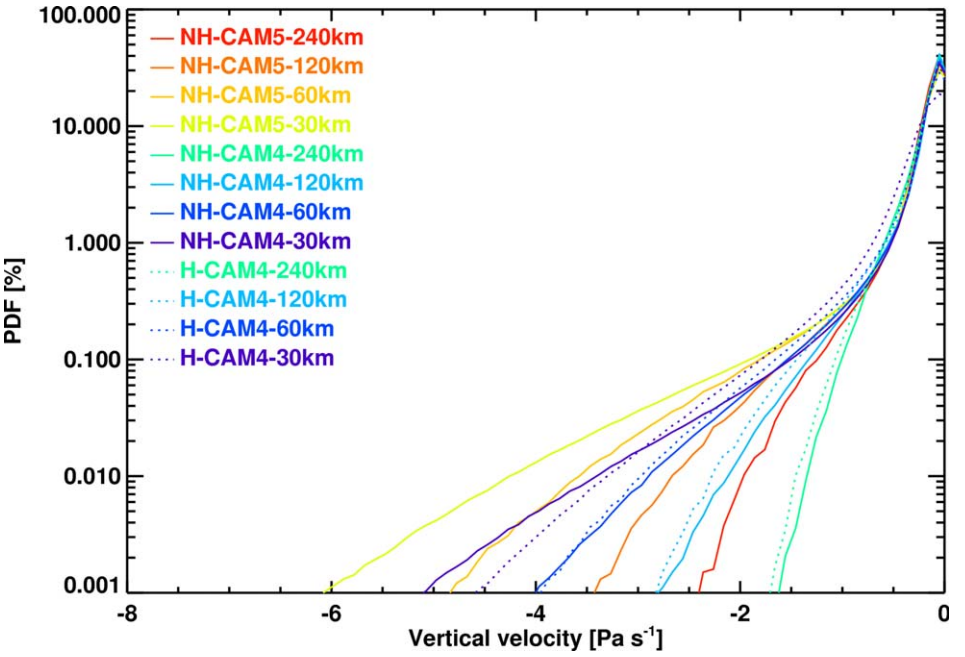

Figure 5. Probability density functions (PDFs) of 6 hourly tropical (10°S–10°N) upward vertical velocity averaged below 700 hPa.

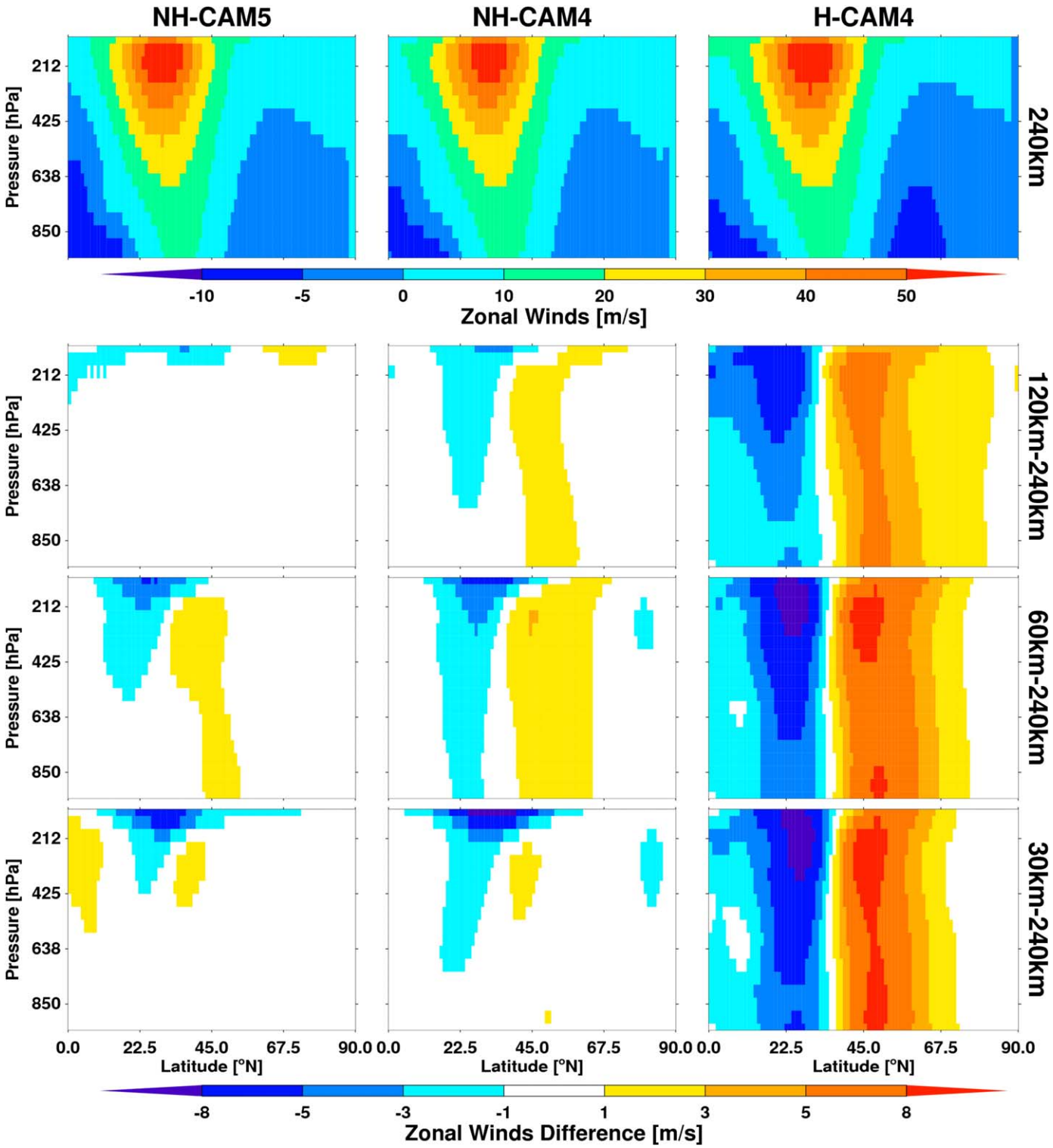

Figure 6. Vertical cross section of zonally averaged zonal winds from the UR NH-MPAS simulations with CAM5 and CAM4 physics and the H-MPAS-CAM4 simulations at 240 km, and the difference between 240 km and three different resolutions of approximately 30, 60, and 120 km.

[2013]. All simulations produce low-level tropical easterlies equatorward of 23°N/S and a single core for the westerly jet at ~200 hPa and ~30°N/S. From the H-MPAS-CAM4 simulations, *Rauscher et al.* [2013] found that the near-surface westerlies display increasing speed with increasing resolution while the upper level

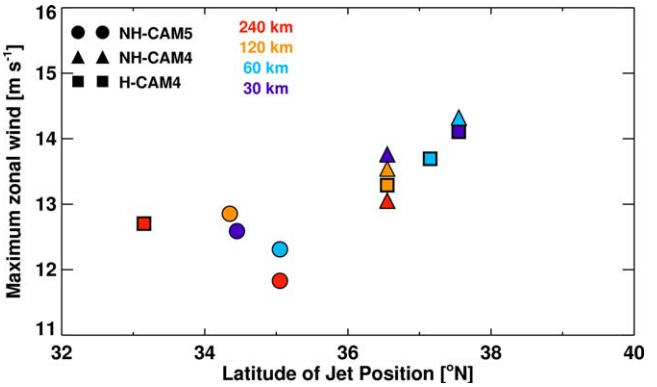

Figure 7. Maximum zonal monthly mean westerly wind speed averaged between 950 and 800 hPa and the corresponding latitude from the UR NH-MPAS simulations with CAM4 and CAM5 physics and the UR H-MPAS-CAM4 simulations at resolutions of 30, 60, 120, and 240 km.

westerlies display decreasing speed with increasing resolution. In this study, the maximum speed of the near-surface (900 hPa) zonally averaged zonal wind varies very little with resolutions from 240 to 30 km, ranging between 13.1 and 13.5 m s^{-1} from NH-MPAS-CAM5 and between 13.9 and 14.3 m s^{-1} from NH-MPAS-CAM4, respectively. Similar small sensitivity of the near surface maximum westerly speed is also found with H-MPAS-CAM4, ranging between 14.0 and 14.4 m s^{-1}. Larger differences between 240 km and other resolutions in H-MPAS than NH-MPAS are mainly due to the poleward shift of the westerlies in H-MPAS that will be further discussed later. The more robust sensitivity across all the experiments with NH-MPAS or H-MPAS is that of the intensity of the upper level (250 hPa) westerly jet to resolution: as the resolution increases from 240 to 30 km, the jet speed decreases from 56.1 to 54.3 m s^{-1} and from 52.6 to 50.0 m s^{-1} in NH-MPAS-CAM5 and NH-MPAS-CAM4, respectively, while it weakens more significantly from 56.7 to 48.5 m s^{-1} in H-MPAS-CAM4. The greater sensitivity found in H-MPAS-CAM4 is more comparable to that in *Rauscher et al.* [2013].

The most recurrent sensitivity about the westerly jet might be its poleward shift with enhanced resolution as reported in many previous studies [*Pope and Stratton*, 2002; *Williamson*, 2008a; *Wan et al.*, 2008; *Lu et al.*, 2015]. The subtropical low level westerly jet position was found to have a large influence on the frequency of atmospheric river events, with lower atmosphere river frequency corresponding to a more poleward placement of the low level westerly jet in H-MPAS-CAM4 [*Hagos et al.*, 2015]. Figure 7 shows the maximum near-surface (900 hPa) zonal mean zonal wind and its corresponding locations (latitudes) from the NH-MPAS simulations with CAM4 and CAM5 physics and the H-MPAS-CAM4 simulations at four different resolutions. Consistent with Figure 6, NH-MPAS with both CAM5 and CAM4 show only small sensitivity in their near surface jet position to resolution, while H-MPAS-CAM4 simulates systematic poleward shifts of the jet position from 33°N to 37.75°N as the mesh size decreases from 240 to 30 km, with the most significant shift occurring between 240 and 120 km. This poleward shift of about 5° between 240 and 30 km with H-MPAS-CAM4 is similar to that reported by *Lu et al.* [2015] for the same model.

To examine the above sensitivity, a finite-amplitude wave activity budget at 250 hPa based on the vorticity equation from *Lu et al.* [2015] is adopted here. This diagnostics links the upper tropospheric eddy vorticity forcing for the eddy-driven jet to the dissipation and the wave activity source. Readers are referred to *Nakamura and Zhu* [2010] for the concept of finite-amplitude wave activity and to *Lu et al.* [2015] for the theoretical framework for the wave activity budget. For brevity, only the eddy vorticity flux, which directly maintains the eddy-driven component of the westerly jet, the wave activity source, and the effective diffusivity are presented for NH-MPAS-CAM5 (Figure 8, upper plots) and NH-MPAS-CAM4 (Figure 8, middle plots), in contrast with the corresponding results for H-MPAS-CAM4 (Figure 8, lower plots). First, one can see that the peaks of the eddy vorticity flux correspond well with the near-surface jet positions shown in Figure 7, indicating that the meridional structure of the latter is maintained by that of the former. As such the eddy vorticity flux exhibits the same sensitivity to model resolution as the jet position. The distinct sensitivities between NH-MPAS and H-MPAS appear to arise from two factors: the different behaviors of the wave activity source, and the different sensitivities of the midlatitude effective diffusivity, which is a measure of the efficiency of the dissipation of wave activity.

To investigate the role of each factor mentioned above, the middle column of Figure 8 shows that in NH-MPAS (for both CAM4 and CAM5 physics), the peak of the wave activity source moves slightly equatorward with increasing resolution, while the opposite is true for H-MPAS-CAM4. Additionally, the NH-MPAS simulations show much weaker sensitivity in the midlatitude effective diffusivity (right column) to resolution than

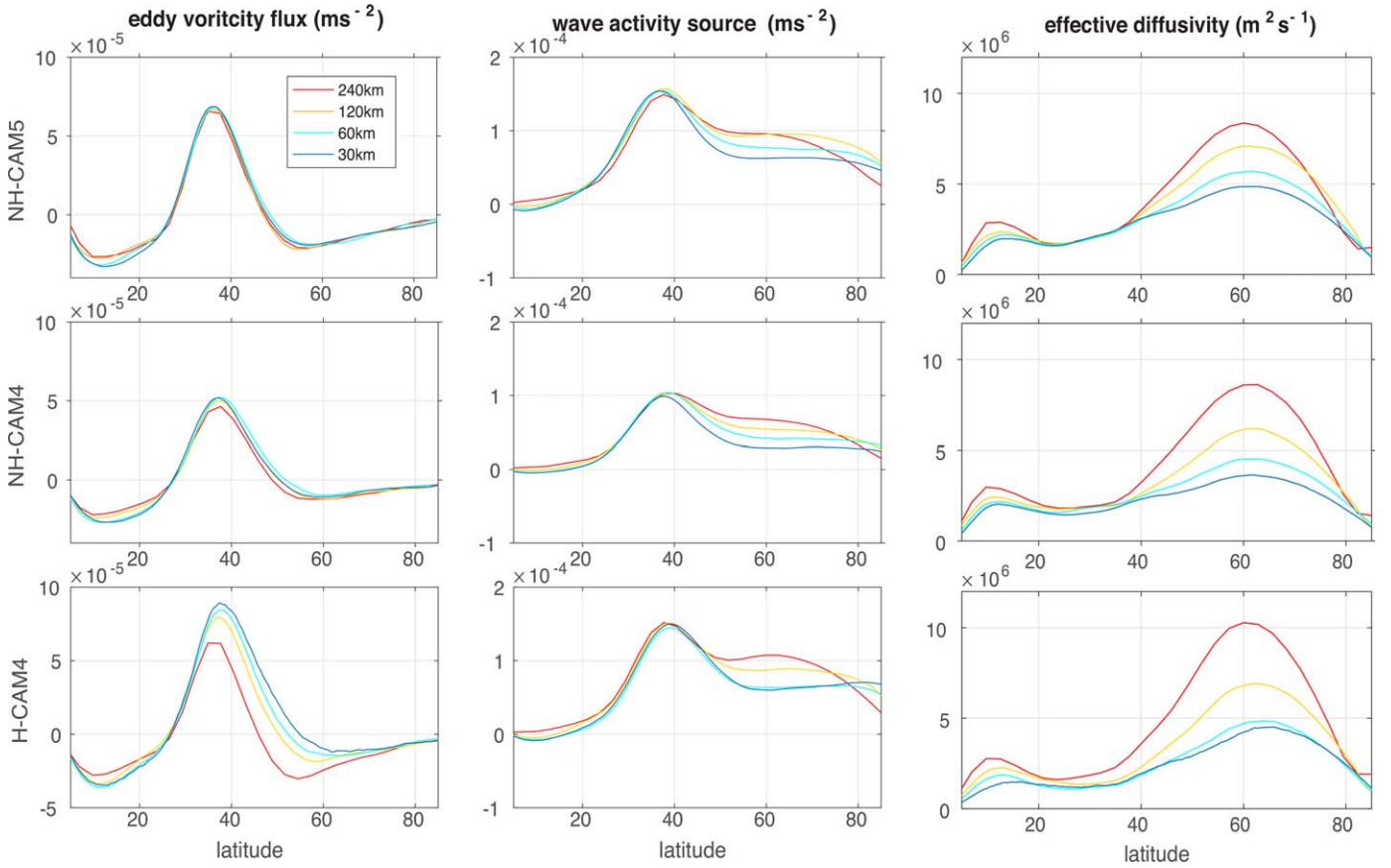

Figure 8. Eddy vorticity flux, wave activity source, and effective diffusivity from the wave activity budget analysis of *Lu et al*. [2015] for the NH-MPAS and H-MPAS simulations at various global quasiuniform resolutions.

the H-MPAS simulations. As discussed in *Lu et al*. [2015], the smaller midlatitude effective diffusivity in higher resolution allows more wave activity to survive the midlatitude dissipation, giving rise to greater meridional propagation of wave activity across the jet and larger eddy vorticity flux (as one can see from comparing the bottom left and bottom right plots in Figure 8). This sensitivity of the effective diffusivity is less acute in NH-MPAS as the resolution increases and the associated mechanism as counterbalance to the weakening and equatorward shift of the wave source is also much weakened. On the other hand, the wave source in H-MPAS-CAM4 tends to shift poleward and the effective diffusivity decreases more drastically with resolution. As a consequence, H-MPAS has a much greater sensitivity in the position of the eddy-driven jet than NH-MPAS. The greater sensitivity of the midlatitude effective diffusivity in H-MPAS than NH-MPAS may be explained by the differences in the hyperdiffusion coefficients used in the corresponding dynamical cores [*Rauscher et al*., 2013; *Park et al*., 2015]. Table 1 shows the hyperdiffusion coefficients among the experiments. The H-MPAS experiments used overall larger coefficients than the NH-MPAS experiments for the same mesh spacing, and the corresponding ratio of the coefficients between H-MPAS and NH-MPAS decreases with increasing resolution. Thus, from the lowest to the highest resolution the hyperdiffusivity decreases with a much greater proportion in H-MPAS than NH-MPAS, which may have contributed to the greater sensitivity of the midlatitude effective diffusivity in the former (Figure 8). A sensitivity experiment with H-MPAS-CAM4 at 240 km with a smaller hyperdiffusion coefficient shows smaller difference in the midlatitude effective diffusivity between 240 and 120 km (not shown), further supporting the influence of the hyperdiffusion coefficient on the effective diffusivity and wave activity simulated by H-MPAS-CAM4.

3.1.2.2. Hadley Circulation

Previous studies using H-MPAS-CAM4 show some sensitivity of the Hadley circulation strength to model resolution. Using the maximum mean meridional streamfunction as a measure of the Hadley circulation strength [*Oort and Yienger*, 1996; *Mitas and Clement*, 2005], H-MPAS-CAM4 simulates a stronger Hadley

circulation with indices ranging from 1.86 to 2.52 ($\times 10^{11}$ kg s^{-1}) with increasing resolution from 240 to 30 km, which is mainly due to the low value (1.86 $\times$ 10^{11} kg s^{-1}) at 240 km. NH-MPAS with CAM5 and CAM4 physics simulates smaller sensitivity of the Hadley circulation strength to resolution with indices ranging between 2.63–2.70 ($\times 10^{11}$ kg s^{-1}) and 2.24–2.43 ($\times 10^{11}$ kg s^{-1}), respectively. CAM5 simulates a slightly stronger Hadley circulation than CAM4. To better understand this resolution impact on the Hadley circulation, we compute the Normalized Gross Moist Stability (NGMS) [see *Raymond et al.*, 2007, 2009]. NGMS relates the relative vertically integrated divergence of moist static energy (h, formally moist entropy, but they are approximately equivalent) to the vertically integrated divergence of water vapor (q). At steady state, this ratio is equivalent to the fluxes of energy and moisture through the top of atmosphere and surface.

$$\text{NGMS} = -\frac{\langle \nabla \cdot h\vec{v} \rangle}{\langle \nabla \cdot q\vec{v} \rangle} = \frac{F_s - R}{P - E}$$

In the equation above, $\vec{v}$ is the wind vector, L_v is the latent heat, F_S is the surface flux of energy (sensible plus latent), R is the integrated radiative sink of energy from the atmosphere, P is the surface precipitation, E is the surface evaporation, and $\langle \bullet \rangle$ denotes a pressure integral from the surface to the top of the atmosphere. Note that precipitation and evaporation on the right-hand side of the equation above are in units of W m^{-2} so that NGMS remains dimensionless. While NGMS is commonly computed using the circulation to make predictions for precipitation, here we compute it using the TOA and surface fluxes to predict the circulation changes. If we neglect the role of eddies and assume that the structure of h and q is relatively constant between simulations (as one might expect for a fixed moist adiabatic temperature profile with fixed relative humidity), then we expect a stronger circulation for a weaker NGMS owing to the fact that the divergence of humidity term grows much faster than the divergence of energy with circulation intensification.

We compute NGMS over the tropical rain band where P is larger than E ($P - E > 0$; the upwelling region of the Hadley circulation). The change in NGMS from 240 to 30 km resolution is -0.025, -0.009, and -0.066 for NH-MPAS-CAM5, NH-MPAS-CAM4, and H-MPAS-CAM4, respectively. From above, the changes in maximum streamfunction are 0.07, 0.19, and 0.66 (all $\times 10^{11}$ kg s^{-1}) for NH-MPAS-CAM5, NH-MPAS-CAM4, and H-MPAS-CAM4, respectively. Both the difference in NGMS and the difference in maximum streamfunction are more than doubled in the H-MPAS-CAM4 experiment compared to NH-MPAS with CAM5 and CAM4 (see Figure 9). NGMS is influenced by changes either in the water cycle ($P - E$) or in the energy fluxes ($F_S - R$). We find here that the energy fluxes are relatively constant with changing resolution, such that increases in $P - E$ (which are dominated by changes in precipitation; not shown) are the dominant control on the decreases in NGMS, and hence the increases in circulation strength. Figure 9 shows that increases in

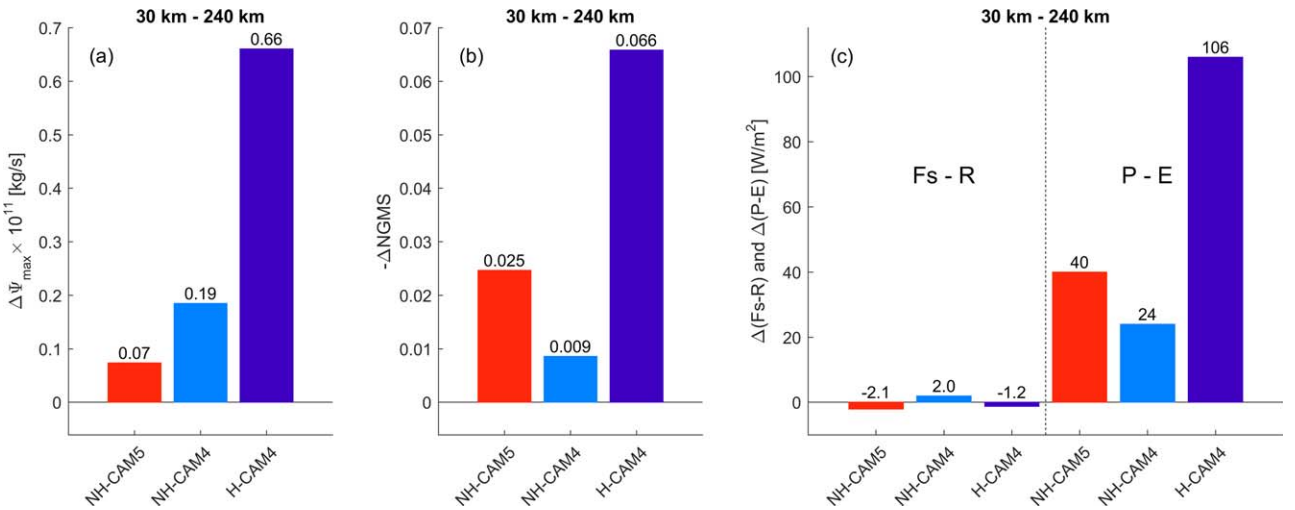

Figure 9. Differences between experiments with 30 km horizontal resolution and 240 km horizontal resolution for: (a) maximum streamfunction, (b) NGMS, and (c) $F_S - R$ (left side) and $P - E$ (right side). The changes in NGMS, $F_S - R$, and $P - E$ are all averaged over the tropical rain band (defined here as the region where $P - E > 0$). Note that we have flipped the signs for ΔNGMS since increasing resolution decreases NGMS in all experiments.

$P - E$ with resolution mimic the increases in streamfunction strength and decreases in NGMS, while changes in $F_S - R$ do not. For NH-MPAS-CAM5, NH-MPAS-CAM4, and H-MPAS-CAM4, the changes in $P - E$ are 40, 24, and 106 W m^{-2}, respectively, while the changes in energy fluxes are only -2.1, 2.0, and -1.2 W m^{-2}, respectively. The different resolution impacts between NH-MPAS and H-MPAS are primarily associated with the differences in relative humidity and resolved vertical velocity profiles (not shown) that influence the cloud microphysical processes and precipitation. Since the energy fluxes at the top of the atmosphere and surface are insensitive to the resolution changes, the NGMS framework shows that Hadley circulation strength increases in the models are coupled to the increases in precipitation.

3.2. Global Variable Resolution Simulations

3.2.1. Precipitation

Figure 10 shows the spatial distribution of the difference in average total, parameterized convective, and resolved large-scale precipitation between the UR MPAS simulations at 30 and 120 km mesh spacing and between the VR (30–>120 km) and UR (120 km) simulations with CAM4 and CAM5 physics. All the simulation results are remapped to a 1 degree grid. Since precipitation and its sensitivity to resolutions beyond 60°N/S are subtle, only results between 60°N/S are shown. The values of tropical precipitation averaged over the refined region (10°S–10°N, 30°W–30°E) from all simulations are summarized in Table 2. As discussed above, all simulations at UR 30 km produce more large-scale and less convective tropical precipitation than those at UR 120 km, with negligible (0.08 mm d^{-1}) and small (0.43 mm d^{-1}) difference in zonal mean tropical total precipitation in NH-MPAS-CAM5 and NH-MPAS-CAM4, respectively. In general, the VR simulations produce comparable resolution impacts on convective and large-scale precipitation in the refined region (black circle) as displayed in the UR 120 and 30 km simulations. The average convective (large-scale) precipitation in the refined region of VR is reduced (enhanced) by -1.48 and -0.31 mm d^{-1} (1.49 and 0.63 mm d^{-1}) in NH-MPAS CAM5 and CAM4, respectively, compared to the corresponding UR 120 km simulations. These changes are comparable to those between UR 30 km and UR 120 km. The sensitivity of convective and large-scale precipitation to model resolution using CAM5 is larger than that using CAM4 as discussed before. H-MPAS-CAM4 also simulates an evident reduction (enhancement) of convective (large-scale) precipitation in the refined region from UR 120 km to VR 30–>120 km. The averaged total precipitation in the refined region is insensitive (changing within 5%) to the resolution change from 120 to 30 km in all simulations.

Similar to the findings from *Rauscher et al*. [2013] and *Hagos et al*. [2013], H-MPAS-CAM4 simulates a zonally asymmetric distribution of resolution impacts on total precipitation in the refined region. That is, despite the smaller changes in total precipitation with resolution in the refined region compared to previous studies, there is still an evident increase of precipitation on the western (downwind) side and decrease on the eastern (upwind) side of the refined region. This asymmetric distribution is mainly due to the asymmetric enhancement and reduction of the large-scale and convective precipitation, respectively, associated with the advection of atmospheric state from the upstream low-resolution region into the refined region. In comparison, NH-MPAS CAM5 and CAM4 simulate a zonally symmetric distribution of resolution impact, a small increase (∼3%) of total precipitation over both sides of the refined region. This results in smaller diabatic heating and streamfunction anomalies compared to those found in *Rauscher et al*. [2013] and *Hagos et al*. [2013] (not shown). The zonally asymmetric precipitation sensitivity to resolutions and the associated circulation anomalies have been attributed to the response of the moist physics to local mesh refinement, which is confirmed by the Held-Suarez [*Held and Suarez*, 1994] test, in which model physics are replaced by prescribed forcing and dissipation [*Rauscher et al*., 2013].

Of interest in the NH-MPAS-CAM4 VR simulation is that the same moist physics (CAM4) coupled to different dynamical cores (NH-MPAS versus H-MPAS) produces a zonally symmetric resolution impact inside the refined region. It is also noteworthy that with a spectral element hydrostatic dynamical core coupled to the CAM4 and CAM5 physics and a pressure-based vertical coordinate, *Zarzycki et al*. [2014] also found zonally symmetric distributions of precipitation changes with resolutions in the refined region. In their study as well as in ours, the moist physics appears to respond to model resolution changes more rapidly across the transition zone. One reason for this may be due to the lower sensitivity of NH-MPAS simulated integrated water vapor (IWV) to resolution. The resolution impacts on IWV averaged over the refined region from NH-MPAS CAM5 and CAM4 (-0.50 and -1.09 mm, respectively) are smaller than that (-1.47 mm) from H-MPAS-CAM4. Averaged near the equator over the refined region (5°S–5°N, 30°W-30°E), a resolution change from

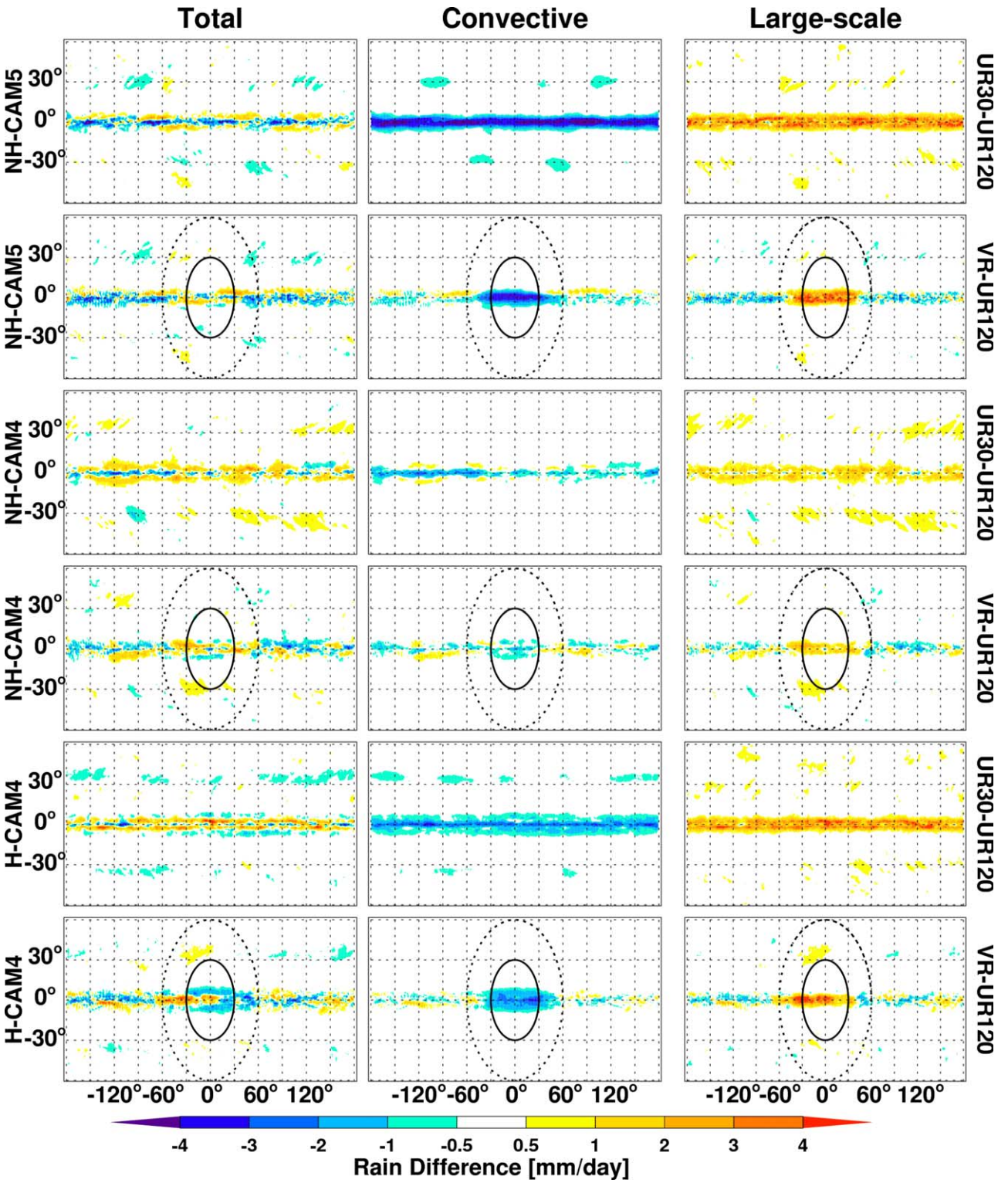

Figure 10. Spatial distribution of the difference in averaged total, parameterized convective, and resolved large-scale precipitation between the MPAS simulations at UR 30 km (UR 30) and 120 km (UR 120) resolutions and between the VR 30–>120 km (VR) and UR 120 resolutions with CAM4 and CAM5 physics. The results are shown between 60°N/S. The black solid line circle denotes the refined region with a radius of 30°. The area between the black solid circle and black dashed circle denotes the transition zone between the refined region and the boundary of coarse resolution with a radius of 60°.

Table 2. Tropical Precipitation Averaged Over the Refined Region (10°S–10°N, 30°W–30°E) for NH-MPAS and H-MPAS at 30, 120, and 30–>120 km

	Total (mm d^{-1})			Convective (mm d^{-1})			Large-Scale (mm d^{-1})		
Model	30 km	120 km	30–>120 km	30 km	120 km	30–>120 km	30 km	120 km	30–>120 km
NH-MPAS-CAM5	9.40	9.48	9.51	4.46	5.93	4.45	4.94	3.56	5.05
NH-MPAS-CAM4	8.69	8.26	8.58	4.96	5.12	4.81	3.73	3.14	3.77
H-MPAS-CAM4	8.92	8.98	8.64	3.35	4.55	3.15	5.57	4.43	5.48

120 to 30 km increases the near-surface (below 700 hPa) vertical velocity slightly by about -0.002 Pa s^{-1} in the NH-MPAS CAM5 and CAM4 simulations, but the impact on the H-MPAS-CAM4 simulated vertical velocity is even smaller. These suggest that the smaller sensitivity of IWV rather than vertical velocity with resolution in the NH-MPAS simulations contribute to the zonally symmetric distribution of precipitation changes in the refined region, which is in stark contrast to the asymmetric distribution simulated in H-MPAS.

3.2.2. Clouds

The monotonic decrease of cloud fraction with increasing horizontal grid resolution is a well-known issue with the CAM physics [e.g., *Williamson*, 2008a, 2008b; *Rauscher et al*., 2013; *O'Brien et al*., 2013; *Zarzycki et al*., 2014]. The increased updraft velocity with increasing resolution (Figure 5) and mass continuity imply that masses are transported upward through narrow columns, therefore reducing the fractional area covered by clouds. *O'Brien et al*. [2013] and *Zarzycki et al*. [2014] found smaller sensitivity of the simulated cloud fraction to resolutions in CAM5 compared to CAM4. Figure 11 shows the spatial distributions of cloud fraction from the MPAS UR 30 and 120 km simulations and the VR simulations. NH-MPAS with CAM4 and CAM5 both display smaller cloud fraction in UR 30 km compared to UR 120 km. The cloud fraction in the refined region of the VR simulations is also smaller than that of the low-resolution region and comparable to that of UR 30 km. Consistent with previous studies [*O'Brien et al*., 2013; *Zarzycki et al*., 2014], CAM5 produces larger cloud fraction than CAM4, and simulates less sensitivity of cloud fraction to resolution. Averaged over the refined region at 30 km, NH-MPAS-CAM5 simulates cloud fraction (0.62) higher than that (0.28) from NH-MPAS-CAM4. In the meantime, the 15% reduction of cloud fraction (0.73–0.62) from 120 to 30 km averaged over the refined region in NH-MPAS-CAM5 is less than the 35% reduction (0.43–0.28) in NH-MPAS-CAM4. H-MPAS-CAM4 simulates a similar reduction of cloud fraction as NH-MPAS-CAM4 but with a larger cloud fraction value of 0.35. Similar to the precipitation response, H-MPAS-CAM4 simulates a zonally asymmetric distribution of cloud fraction reduction between the eastern and western sides of the refined region. As with precipitation, such behavior is not apparent in the NH-MPAS simulations with either CAM4 or CAM5 physics.

4. Summary and Discussion

This study analyzed a series of aqua-planet simulations conducted using NH-MPAS with the CAM4 and CAM5 physics to document the distinct simulated features of precipitation, clouds, and large-scale circulation compared to behaviors reported in previous studies for H-MPAS-CAM4. Similar to previous studies [e.g., *Rauscher et al*., 2013], the quasiuniform resolution experiments show large reductions in the ratio of convective to large-scale precipitation with increasing model resolution related to the sensitivity of large-scale condensation from the cloud microphysics to the resolved vertical velocities. This ratio has larger sensitivity in NH-MPAS-CAM5 than NH-MPAS-CAM4. Compared to H-MPAS-CAM4, NH-MPAS-CAM4 generally simulates more convective precipitation and less large-scale precipitation at all resolutions but their sensitivities to resolution are comparable. Despite the apparent sensitivity of each precipitation component to resolution, sensitivity of the total precipitation to resolution is very small, particularly for NH-MPAS-CAM5.

As model resolution increases, all models produced higher frequencies of more intense precipitation with no sign of convergence even when the simulations are all interpolated to the same coarser resolution grid. CAM5 has a propensity to produce more intense precipitation than CAM4. This is consistent with the changes of extreme upward vertical velocity to resolution. Although the differences are small, NH-MPAS-CAM4 consistently produces slightly lower frequencies of intense precipitation than H-MPAS-CAM4, which may be related to the treatment of vertical velocity that is diagnosed in H-MPAS and predicted in NH-MPAS. Thus in H-MPAS, the positive feedback between latent heating from large-scale condensation produced by

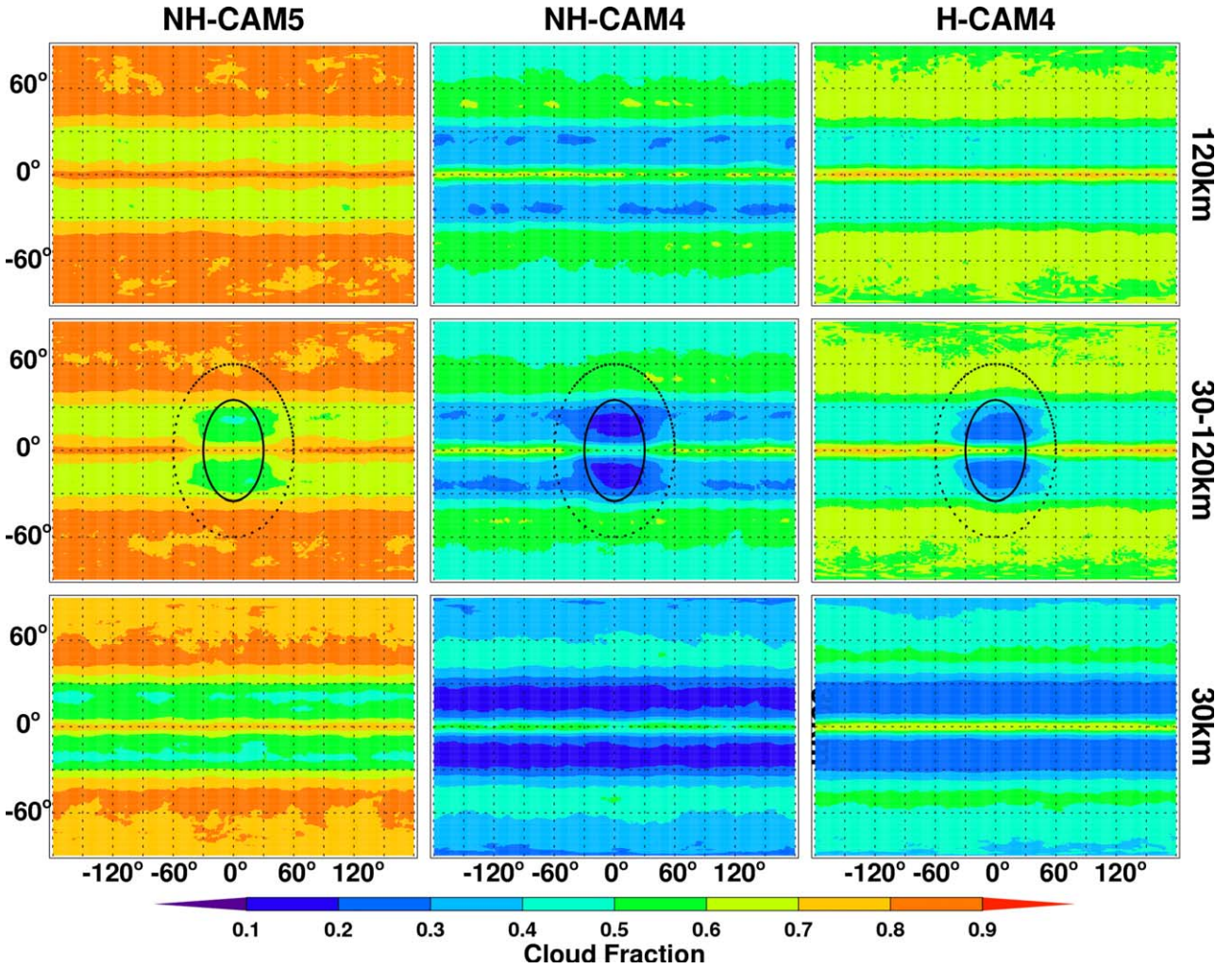

Figure 11. Spatial distributions of cloud fraction from the MPAS UR simulations at 30 and 120 km and the VR simulations at 30–>120 km in different experiments. The results are shown between 90°N/S. The black solid circle denotes the refined region with a radius of 30°. The black dashed circle denotes the boundary of the coarse resolution region with a radius of 60°.

cloud microphysics and the vertical velocity may be stronger because the adjustment of the vertical velocity to the latent heating is instantaneous based on diagnostic relationships. Note that the same physics and dynamics time steps as well as moist physics parameters are used in all experiments so the different model sensitivities can be attributed to differences in the dynamical cores or physics parameterizations rather than time steps and convective time scales, as discussed in *Williamson* [2013].

The NH-MPAS and H-MPAS simulations display significantly different sensitivity of large-scale circulation features to model resolution. The most notable difference is the simulated structure of the ITCZ: instead of a transition from single to double ITCZ in previous simulations as model resolution increases, our simulations show an unambiguous single ITCZ at all resolutions examined. With a well-balanced global moisture budget, NH-MPAS with CAM4 or CAM5 physics also produced a single ITCZ at all model resolutions ranging from 240 to 30 km. These findings support the mechanisms identified by *Landu et al.* [2014], where the feedback between convection and large-scale circulation is differentiated by the influence of atmospheric moisture content on CAPE (which is lower in the previous H-MPAS-CAM4 simulations) and the parameterized convection in the simulations.

From analysis of the westerly jet and Hadley circulation, NH-MPAS also displays much lower sensitivity to model resolution than H-MPAS. *Lu et al.* [2015] found that the low level westerly jet shifts poleward with increasing resolution in H-MPAS-CAM4, which also significantly affects the simulated frequency of atmospheric river events [*Hagos et al.*, 2015]. The H-MPAS-CAM4 simulations in this study show similar results,

but the jet position simulated by NH-MPAS CAM5 and CAM4 is almost insensitive to horizontal resolutions. The difference is mainly attributable to the poleward shift of the peaks of eddy vorticity flux with increasing resolution in H-MPAS-CAM4, which is forced by a poleward shift of the wave activity source as well as a larger reduction in effective diffusivity with increasing resolution, thus more wave activity survives the midlatitude dissipation as the resolution increases. On the contrary, the NH-MPAS simulations show an equatorward shift of the wave activity source and smaller reductions in effective diffusivity with increasing resolution. The different resolution sensitivity between NH-MPAS and H-MPAS is partly related to the hyperdiffusivity used in the two dynamical cores. The sensitivity of the Hadley circulation strength to resolution simulated by NH-MPAS is similar between CAM4 and CAM5, and is weaker than H-MPAS with CAM4. The diagnosis of NGMS shows that the increase in the hydrologic cycle with increasing resolutions, apart from energy fluxes, dominates the increase in Hadley circulation strength. The NGMS diagnostic confirms that the lower sensitivity of the Hadley circulation to resolution in NH-MPAS compared to H-MPAS can be attributed to the lower sensitivity of the tropical total precipitation in the former.

Lastly, we analyzed the VR simulations for the three models with different dynamical cores and physics parameterizations. The averaged total precipitation over the refined region is much less sensitive to the resolution change from 120 to 30 km in all experiments compared to previous studies. Therefore, the magnitude of anomalous rotational flow at 200 hPa that is driven by the anomalous heating over the refined region is also much weaker than previous studies [e.g., *Rauscher et al*., 2013; *Hagos et al*., 2013]. Despite the reduced sensitivity of precipitation to resolution, the simulated cloud fraction still significantly decreases with increasing resolution in the UR simulations and over the refined region in the VR simulations. Consistent with previous studies [*O'Brien et al*., 2013; *Zarzycki et al*., 2014], CAM5 produces larger cloud fraction and is less sensitive than CAM4 to resolutions. H-MPAS-CAM4 in this study still simulates an asymmetric distribution of resolution impacts on total precipitation over the refined region, as noted in *Rauscher et al*. [2013] and *Hagos et al*. [2013]. In contrast, NH-MPAS simulates a symmetric distribution of resolution impact over the refined region, which is consistent with what *Zarzycki et al*. [2014] found using a spectral element hydrostatic dynamical core and CAM4 and CAM5 physics. We found lower sensitivity of IWV in NH-MPAS transitioning from the low to the high-resolution region than in H-MPAS. Correspondingly, NH-MPAS-CAM4 also simulates a symmetric distribution of cloud fraction in the refined region, in contrast to H-MPAS that simulates an asymmetric distribution.

Overall, this study reveals a lower sensitivity in NH-MPAS to horizontal resolution compared to H-MPAS in many climatic features. This provides benefits to the VR configuration for producing more zonally symmetric features that are more comparable to the UR simulations in an aqua-planet framework. The differences between NH-MPAS and H-MPAS are related to differences in the dynamical cores, including the nonhydrostatic versus hydrostatic formulations, differences in vertical coordinates and vertical resolutions, differences in hyperdiffusion coefficients, and other features. The differences between the CAM4 and CAM5 simulations may be partly a result of different cloud microphysics and boundary layer schemes. Our analyses show that important differences in humidity and precipitation can result from differences in the formulation of the dynamical cores alone, which have notable effects on the tropical large-scale circulation features including the ITCZ and Hadley circulation. Given the strong coupling between dynamics and physics, more in-depth analyses and numerical experiments are needed to disentangle the physical mechanisms governing any specific process presented in this paper. The reduced resolution sensitivity of NH-MPAS demonstrated in this study should motivate future research to further investigate the model behaviors and explore its use in very high resolution and convection-permitting simulations using regional refinement.

Acknowledgments

This research was supported by the Office of Science of the U.S. Department of Energy (DOE) as part of the Regional & Global Climate Modeling (RGCM) program. Dr. J.-H. Yoon was partially supported by funding from the Korean Polar Research Institute. This study used computing resources from the National Energy Research Scientific Computing Center, which is the DOE Office of Science User Facility supported by the Office of Science of the U.S. Department of Energy under contract DE-AC02-05CH11231 and contract DE-AC02-06CH11357, respectively. Pacific Northwest National Laboratory is operated by Battelle Memorial Institute for the DOE under contract DE-AC05-76RL01830.

References

Bacmeister, J. T., M. F. Wehner, R. B. Neale, A. Gettelman, C. Hannay, P. H. Lauritzen, J. M. Caron, and J. E. Truesdale (2014), Exploratory high-resolution climate simulations using the Community Atmosphere Model (CAM), *J. Clim.*, *27*, 3073–3099, doi:10.1175/JCLI-D-13-00387.1.

Du, Q., V. Faber, and M. Gunzburger (1999), Centroidal Voronoi tessellations: Applications and algorithms, *SIAM Rev.*, *41*(4), 637–676.

Gettelman, A., H. Morrison, and S. J. Ghan (2008), A new two-moment bulk stratiform cloud microphysics scheme in the NCAR Community Atmosphere Model (CAM3), Part II: Single-column and global results, *J. Clim.*, *21*(15), 3660–3679.

Gill, A. E. (1980), Some simple solutions for heat-induced tropical circulation, *Q. J. R. Meteorol. Soc.*, *106*, 447–462.

Giorgi, F., and L. O. Mearns (1991), Approaches to the simulation of regional climate change: A review, *Rev. Geophys.*, *29*(2), 191–216, doi:10.1029/90RG02636.

Giorgi, F., and M. R. Marinucci (1996), An investigation of the sensitivity of simulated precipitation to the model resolution and its implications for climate studies, *Mon. Weather Rev.*, *124*, 148–166, doi:10.1175/1520-0493(1996)124 < 0148:AIOTSO>2.0.CO;2.
Hagos, S., R. Leung, S. A. Rauscher, and T. Ringler (2013), Error characteristics of two grid refinement approaches in aquaplanet simulations: MPAS-A and WRF, *Mon. Weather Rev.*, *141*, 3022–3036, doi:10.1175/MWR-D-12-00338.1.
Hagos, S., L. R. Leung, Q. Yang, C. Zhao, and J. Lu (2015), Resolution and dynamical core dependence of atmospheric river frequency in global model simulations, *J. Clim.*, *28*, 2764–2776, doi:10.1175/JCLI-D-14-00567.1.
Held, I. M., and M. J. Suarez (1994), A proposal for the intercomparison of the dynamical cores of atmospheric general circulation models, *Bull. Am. Meteorol. Soc.*, *75*, 1825–1830.
IPCC (2013), Climate change 2013: The physical science basis, in *The Contribution of Working Group I to the Fifth Assessment Report of the Intergovernmental Panel on Climate Change*, edited by T. F. Stocker et al., Cambridge Univ. Press, Cambridge, U. K.
Ju, L. T., T. Ringler, and M. Gunzburger (2011), Voroni tessellations and their application to climate and global modeling, in *Numerical Techniques for Global Atmospheric Models, vol. 80, Lecture Notes in Computational Science and Engineering*, edited by P. H. Lauritzen et al., pp. 313–342, Springer.
Landu, K., L. R. Leung, S. Hagos, V. Vinoj, S. Rauscher, T. Ringler, and M. Taylor (2014), The dependence of ITCZ structure on model resolution and dynamical core in aquaplanet simulations, *J. Clim.*, *27*, 2375–2385, doi:10.1175/JCLI-D-13-00269.1.
Leung, L. R., L. O. Mearns, F. Giorgi, and R. L. Wilby (2003), Regional climate research, *Bull. Am. Meteorol. Soc.*, *84*, 89–95.
Leung, L. R., T. Ringler, W. D. Collins, and M. Ashfaq (2013), A hierarchical evaluation of regional climate simulations, *Eos Trans. AGU*, *94*, 297–298.
Liu, X., et al. (2012), Toward a minimal representation of aerosols in climate models: Description and evaluation in the Community Atmosphere Model CAM5, *Geosci. Model Dev.*, *5*, 709–739, doi:10.5194/gmd-5-709-2012.
Lu, J., G. Chen, L. R. Leung, D. A. Burrows, Q. Yang, K. Sakaguchi, and S. Hagos (2015), Toward the dynamical convergence on the jet stream in aquaplanet AGCMs, *J. Clim.*, *28*(17), 6763–6782, doi:10.1175/JCLI-D-14-00761.1.
Medvigy, D., R. L. Walko, M. J. Otte, and R. Avissar (2013), Simulated changes in northwest U.S. climate in response to Amazon deforestation, *J. Clim.*, *26*, 9115–9136, doi:10.1175/JCLI-D-12-00775.1.
Mitas, C. M., and A. Clement (2005), Has the Hadley cell been strengthening in recent decades? *Geophys. Res. Lett.*, *32*, L03809, doi:10.1029/2004GL021765.
Morrison, H., and A. Gettelman (2008), A new two-moment bulk stratiform cloud microphysics scheme in the NCAR Community Atmosphere Model (CAM3), Part I: Description and numerical tests, *J. Clim.*, *21*(15), 3642–3659.
Murakami, H., and M. Sugi (2010), Effect of model resolution on tropical cyclone climate projections, *Sci. Online Lett. Atmos.*, *6*, 73–76, doi:10.2151/sola.2010-019.
Murakami, H., et al. (2012), Future changes in tropical cyclone activity projected by the new high-resolution MRI-AGCM*, *J. Clim.*, *25*, 3237–3260, doi:10.1175/JCLI-D-11-00415.1.
Nakamura, N., and D. Zhu (2010), Finite-amplitude wave activity and diffusive flux of potential vorticity in eddy-mean flow interaction, *J. Atmos. Sci.*, *67*, 2701–2716, doi:10.1175/2010JAS3432.1.
Neale, R. B., and B. J. Hoskins (2000), A standard test for AGCMs including their physical parameterizations. I: The proposal, *Atmos. Sci. Lett.*, *1*, 101–107, doi:10.1006/asle.2000.0022.
Neale, R. B., J. H. Richter, A. J. Conley, and S.-J. Lin (2010), Description of the NCAR Community Atmosphere Model (CAM 4.0), *NCAR Tech. Note NCAR/TN-4851STR*. [Available at http://www.cesm.ucar.edu/models/ccsm4.0/cam/docs/description/cam4_desc.pdf.]
Neale, R. B., J. H. Richter, A. J. Conley, and S.-J. Lin (2012), Description of the NCAR Community Atmosphere Model (CAM 5.0), *NCAR Tech. Note NCAR/TN-4851STR*. [Available at http://www.cesm.ucar.edu/models/cesm1.0/cam/docs/description/cam5_desc.pdf].
NRC (2012), *National Research Council Board, A National Strategy for Advancing Climate Modeling*, The Natl. Acad. Press, Washington, D. C. [Available at http://www.nap.edu/catalog/13430/a-national-strategy-for-advancing-climate-modeling].
O'Brien, T. A., F. Li, W. D. Collins, S. A. Rauscher, T. D. Ringler, M. Taylor, S. M. Hagos, and L. R. Leung (2013), Observed scaling in clouds and precipitation and scale incognizance in regional to global atmospheric models, *J. Clim.*, *26*, 9313–9333, doi:10.1175/JCLI-D-13-00005.1.
Oort, A. H., and J. J. Yienger (1996), Observed interannual variability in the Hadley circulation and its connection to ENSO, *J. Clim.*, *9*, 2751–2767.
Park, S., and C. S. Bretherton (2009), The University of Washington shallow convection and moist turbulence schemes and their impact on climate simulations with the community atmosphere model, *J. Clim.*, *22*, 3449–3469.
Park, S. H., W. C. Skamarock, J. B. Klemp, L. D. Fowler, and M. G. Duda (2013), Evaluation of global atmospheric solvers using extensions of the Jablonowski and Williamson baroclinic wave test case, *Mon. Weather Rev.*, *141*, 3116–3129, doi:10.1175/MWR-D-12-00096.1.
Park, S.-H., W. C. Skamarock, and P. Laurtizen (2015), Impact of vertical resolution using variable-resolution CAM-MPAS, Abstract A51J-0202 presented at 2015 Fall Meeting, AGU, San Francisco, Calif., 14–18 Dec.
Pope, PV. D., and R. A. Stratton (2002), The processes governing horizontal resolution sensitivity in a climate model, *Clim. Dyn.*, *19*, 211–236, doi:10.1007/s00382-001-0222-8.
Rasch, P. J., and J. E. Kristjánsson (1998), A comparison of the CCM3 model climate using diagnosed and predicted condensate parameterizations, *J. Clim.*, *11*, 1587–1614.
Rauscher, S. A., T. D. Ringler, W. C. Skamarock, and A. A. Mirin (2013), Exploring a global multiresolution modeling approach using aquaplanet simulations, *J. Clim.*, *26*, 2432–2452, doi:10.1175/JCLI-D-12-00154.1.
Raymond, D. J., S. L. Sessions, and Ž. Fuchs (2007), A theory for the spinup of tropical depressions, *Q. J. R. Meteorol. Soc.*, *1754*, 1743–1754, doi:10.1002/qj.125.
Raymond, D. J., S. L. Sessions, A. H. Sobel, and Ž. Fuchs (2009), The mechanics of gross moist stability, *J. Adv. Model. Earth Syst.*, *1*, 9, doi:10.3894/JAMES.2009.1.9.
Ringler, T., L. Ju, and M. Gunzburger (2008), A multiresolution method for climate system modeling: Application of spherical centroidal Voronoi tessellations, *Ocean Dyn.*, *58*, 475–498, doi:10.1007/s10236-008-0157-2.
Ringler, T., J. Thuburn, J. B. Klemp, and W. C. Skamarock (2010), A unified approach to energy conservation and potential vorticity dynamics for arbitrarily structured C-grids, *J. Comput. Phys.*, *229*, 3065–3090, doi:10.1016/j.jcp.2009.12.007.
Ringler, T., D. Jacobsen, M. Gunzberger, L. Ju, M. Duda, and W. Skamarock (2011), Exploring a multiresolution modeling approach within the shallow-water equations, *Mon. Weather Rev.*, *139*, 3348–3368.
Roberts, M. J., P. L. Vidale, M. S. Mizielinski, M. E. Demory, R. Schiemann, J. Strachan, K. Hodges, R. Bell, and J. Camp (2015), Tropical cyclones in the upscale ensemble of high resolution global climate models, *J. Clim.*, *28*, 574–596, doi:10.1175/JCLI-D-14-00131.1.
Sakaguchi K., L. R. Leung, C. Zhao, Q. Yang, J. Lu, S. M. Hagos, S. Rauscher, L. Dong, T. Ringler, and P. H. Lauritzen (2015), Exploring a multiresolution approach using AMIP simulations, *J. Clim.*, *28*(14), 5549–5574, doi:10.1175/JCLI-D-14-00729.1.

Skamarock, W. C., J. B. Klemp, J. Dudhia, D. O. Gill, D. M. Barker, X.-Y. Huang, W. Wang, and J. G. Powers (2008), A description of the Advanced Research WRF version 3, *NCAR Tech. Note NCAR/TN-4751STR*, 113 pp.

Skamarock, W. C., J. B. Klemp, L. D. Fowler, M. G. Duda, S.-H. Park, and T. D. Ringler (2012), A multiscale nonhydrostatic atmospheric model using centroidal Voronoi tesselations and C-grid staggering, *Mon. Weather Rev.*, *140*, 3090–3105, doi:10.1175/MWR-D-11-00215.1.

Skamarock, W. C., S.-H. Park, J. B. Klemp, and C. Snyder (2014), Atmospheric kinetic energy spectra from global high-resolution nonhydrostatic simulations, *J. Atmos. Sci.*, *71*, 4369–4381, doi:10.1175/JAS-D-14-0114.1.

Thuburn, J., T. D. Ringler, W. C. Skamarock, and J. B. Klemp (2009), Numerical representation of geostrophic modes on arbitrarily structured C-grids, *J. Comput. Phys.*, *228*, 8321–8335.

Wan, H., M. A. Giorgetta, and L. Bonaventura (2008), Ensemble Held-Suarez test with a spectral transform model: Variability, sensitivity, and convergence, *Mon. Weather Rev.*, *136*, 1075–1092, doi:10.1175/2007MWR2044.1.

Wang, Y., L. R. Leung, J. L. McGregor, D. K. Lee, W. C. Wang, Y. Ding, and F. Kimura (2004), Regional climate modeling: Progress, challenges, and prospects, *J. Meteorol. Soc. Jpn.*, *82*(6), 1599–1628.

Wehner, M. F., et al. (2014), The effect of horizontal resolution on simulation quality in the Community Atmospheric Model, CAM5.1, *J. Adv. Model. Earth Syst.*, *6*(4), 980–997, doi:10.1002/2013MS000276.

Wehner, M. F., Prabhat, K. A. Reed, D. Stone, W. D. Collins, and J. T. Bacmeister (2015), Resolution dependence of future tropical cyclone projections of cam5.1 in the US CLIVAR Hurricane Working Group idealized group idealized configurations, *J. Clim.*, *28*, 3905–3925, doi:10.1175/JCLI-D-14-00311.1.

Williamson, D. L. (2008a), Convergence of aqua-planet simulations with increasing resolution in the Community Atmospheric Model, version 3, *Tellus, Ser. A*, *60*, 848–862.

Williamson, D. L. (2008b), Equivalent finite volume and Eulerian spectral transform horizontal resolutions established from aqua-planet simulations, *Tellus, Ser. A*, *60*, 839–847.

Williamson, D. L. (2013), The effect of time steps and time-scales on parameterization suites, *Q. J. R. Meteorol. Soc.*, *139*(January), 548–560, doi:10.1002/qj.1992.

Williamson, D. L., J. Drake, J. Hack, R. Jakob, and P. Swarztrauber (1992), A standard test set for numerical approximations to the shallow water equations in spherical geometry, *J. Comput. Phys.*, *102*, 211–224.

Yang, Q., L. R. Leung, S. A. Rauscher, T. D. Ringler, and M. A. Taylor (2014), Atmospheric moisture budget and spatial resolution dependence of precipitation extremes in aquaplanet simulations, *J. Clim.*, *27*, 3565–3581, doi:10.1175/JCLI-D-13-00468.1.

Zarzycki, C. M., M. N. Levy, C. Jablonowski, J. R. Overfelt, M. A. Taylor, and P. A. Ullrich (2014), Aquaplanet experiments using CAM's variable-resolution dynamical core, *J. Clim.*, *27*, 5481–5503, doi:10.1175/JCLI-D-14-00004.1.

Zhang, G. J., and N. A. McFarlane (1995), Sensitivity of climate simulations to the parameterization of cumulus convection in the Canadian Climate Centre general circulation model, *Atmos. Ocean*, *33*, 407–446.

Zhang, M., W. Lin, C. S. Bretherton, J. J. Hack, and P. J. Rasch (2003), A modified formulation of fractional stratiform condensation rate in the NCAR community atmospheric model (CAM2), *J. Geophys. Res.*, *108*(D1), 4035, doi:10.1029/2002JD002523.